Proceedings of CONF-FMCE 2025 Symposium: Semantic Communication for Media Compression and Transmission
DOI: 10.54254/2755-2721/2025.GL29304

Nano Silicon-Carbon Composites for Lithium-Ion Battery Applications

Yuxiang Xia

School of Natural Sciences, The University of Manchester, Manchester, United Kindom
yuxiang.xia@student.manchester.ac.uk

Abstract. Silicon-carbon (Si-C) composites are promising replacements for graphite anodes but must deliver high areal loading and durability under lean-electrolyte, full-cell conditions. This work benchmarks three architectures, (i) amorphous-carbon shells with curved planes and strong sp^3 anchoring (a-C:FL), (ii) graphene/pitch-carbon shells formed by spray-drying and thermal treatment, and (iii) sputtered Si on free-standing CNT fabrics, through a unified structure-interface-manufacturability lens. We relate carbon topology and shell chemistry to interfacial impedance, initial coulombic efficiency (ICE), rate capability, and fade mechanisms, while assessing scale-up compatibility. a-C:FL yields LiF-rich, low-impedance interphases, crack tolerance, and robust cycling at practical loadings, indicating the most balanced path to manufacturable performance. Graphene/pitch shells boost conductivity and suppress swelling but display capacity/ICE dilution and tap-density penalties that require careful control of graphene fraction, shell thickness, and electrode porosity. CNT fabrics enable simple processing and rapid early efficiency gains yet suffer from non-uniform utilization and large first-cycle loss without conformal deposition and interphase engineering. We recommend prioritizing graded a-C shells coupled with high-solids slurry processing, calendering, and efficient prelithiation, while advancing targeted co-optimization for graphene and CNT routes. These findings chart a practical route from half-cell promise to bankable, high-loading industrial Si-C anodes and motivate hybrid designs that merge the strengths of all three frameworks.

Keywords: Nano-silicon / Silicon-carbon composites, Carbon nanotubes

1. Introduction

In recent years, the global shift towards sustainable transportation and clean energy has significantly accelerated the development of electric vehicles (EVs) and renewable energy storage systems. As a result, the demand for high-performance energy storage solutions has surged, systems that must deliver not only high energy and power densities but also excellent safety, long cycle life, and cost-effectiveness. Lithium-ion batteries (LIBs), due to their superior electrochemical properties such as high energy density, low self-discharge, and long cycling stability, have become the dominant energy source for portable electronics, grid-scale storage, and electric mobility [1]. However, the increasing performance requirements of modern applications are driving LIBs close to their theoretical limits, especially with regard to anode capacity. The most widely used anode material,

© 2026 The Authors. This is an open access article distributed under the terms of the Creative Commons Attribution License 4.0 (https://creativecommons.org/licenses/by/4.0/).

DOI: 10.54254/2755-2721/2025.GL29304

graphite, has a limited theoretical specific capacity of 372 $mAh \cdot g^{-1}$, which restricts the energy density of next-generation batteries [2].

To overcome this limitation, Silicon (Si) has attracted significant attention as a next-generation anode material. Silicon exhibits an exceptionally high theoretical specific capacity of approximately 4200 $mAh \cdot g^{-1}$ (based on full lithiation to $Li_{4.4}Si$), more than ten times higher than that of graphite. It also features a low lithiation potential (<0.5 V vs. Li^+/Li), natural abundance, and environmental benignity, making it an ideal candidate to replace graphite [3]. However, its practical implementation is hindered by two major issues: (1) large volume expansion (up to 300-400%) during lithiation/delithiation, which induces mechanical stress, particle pulverization, and electrode disintegration; and (2) low intrinsic electrical conductivity, which hampers rate capability and results in unstable solid electrolyte interphase (SEI) formation over prolonged cycling [3].

To address these challenges, extensive research has been devoted to two key strategies: reducing silicon to the nanoscale and constructing silicon-carbon (Si/C) composites. Nanostructured silicon can better accommodate volume changes and reduce pulverization by shortening lithium diffusion lengths and improving mechanical flexibility [4]. However, nanoscale Si often suffers from increased surface reactivity, leading to uncontrolled SEI growth. To stabilize the electrode interface, carbon materials are commonly introduced to form Si/C hybrid composites, which serve to buffer volume changes, enhance electronic conductivity, suppress silicon agglomeration, and protect active material through SEI regulation [5]. Structural designs such as yolk-shell and core-shell architectures further enable internal voids to absorb silicon expansion without compromising mechanical integrity [5].

Recent developments have demonstrated the effectiveness of combining nano-silicon with various carbon structures. For example, incorporating vertical graphene nanosheets into yolk-shell structured Si/C composites significantly improves ion/electron transport and structural robustness under long-term cycling [5]. Similarly, amorphous carbon matrices provide a continuous conductive network and buffer the stress generated by Si expansion, while also being scalable and low-cost [1]. Carbon nanotubes (CNTs), owing to their 1D morphology, high tensile strength, and excellent electrical conductivity, have been used to construct 3D conductive frameworks that effectively maintain electrical connectivity during repeated cycles [6,7]. Furthermore, industrially feasible processes using waste silicon and biomass-derived carbons have been proposed, providing an avenue toward scalable and economical production of high-performance Si/C anodes [2]. Therefore, the objective of this paper is to comprehensively examine the design strategies, material architectures, and electrochemical behaviors of various Si/C composite anodes, particularly focusing on three representative carbon materials: amorphous carbon, graphene, and carbon nanotubes. Through a comparative case study of these carbon structures in Si/C systems, the study aims to elucidate their functional contributions to cycle stability, rate performance, and mechanical resilience. Moreover, this work explores the prospects of incorporating these composite structures into low-cost, scalable fabrication routes, aiming to accelerate the commercialization of next-generation LIBs.

This paper is organized as follows: Section 2 introduces specific cases of Si/C composite anodes utilizing amorphous carbon, graphene, and CNTs. Section 3 provides a comparative analysis of electrochemical performance and mechanical properties. Section 4 offers suggestions for future improvements in material design and process integration. Finally, Section 5 concludes with a summary of findings and potential research directions.

DOI: 10.54254/2755-2721/2025.GL29304

2. Case

2.1. Amorphous carbon

Amorphous carbon is a disordered form of carbon that lacks the long-range crystalline structure found in graphite. Its atomic arrangement is typically random, often containing a mixture of sp^2 and sp^3 hybridized carbon atoms. This structural irregularity contributes to several desirable properties for lithium-ion battery applications. Firstly, the inherent porosity of amorphous carbon allows it to accommodate the significant volume expansion of silicon during lithiation and delithiation processes. This buffering capability mitigates particle pulverization and helps preserve the mechanical integrity of the anode structure. Secondly, amorphous carbon generally exhibits sufficient mechanical strength and elasticity, which enhances the electrode's structural resilience under repeated cycling. This ensures that the silicon particles remain embedded in the conductive matrix, thereby maintaining stable electrochemical performance. In addition, the relatively low reactivity of amorphous carbon with the electrolyte reduces the formation of unstable solid electrolyte interphases (SEI), contributing to a higher initial coulombic efficiency and improved long-term stability. Due to its tunable porosity and ease of synthesis, amorphous carbon is often used in scalable fabrication processes and is considered a practical choice for commercial electrode design.

2.2. Graphene

Graphene is a two-dimensional sheet of carbon atoms arranged in a honeycomb lattice. It possesses exceptional electrical conductivity, high surface area, and outstanding mechanical strength, making it an ideal conductive component in silicon-carbon anodes. When used as a composite with silicon, graphene serves multiple functions. It provides a highly conductive network for electron transport, ensuring rapid charge and discharge cycles. Furthermore, its flexible nature allows it to act as a mechanical buffer, accommodating the volume changes of silicon without structural failure. Graphene can also form a protective layer around silicon particles, which helps reduce direct contact between silicon and the electrolyte. This minimizes undesirable side reactions and stabilizes the SEI layer over multiple charge-discharge cycles. Additionally, the large specific surface area of graphene enhances active material dispersion and facilitates uniform lithium-ion flux during electrochemical processes. Variants such as reduced graphene oxide (rGO) are commonly used due to their processability and ability to form strong interactions with silicon particles. Graphene-based composites are often engineered into layered or interconnected structures to improve both conductivity and mechanical stability.

2.3. Carbon Nanotubes (CNTs)

Carbon nanotubes are cylindrical nanostructures formed by rolling graphene sheets into tubular shapes. They can be categorized into single-walled (SWCNTs) and multi-walled (MWCNTs) types, both offering high aspect ratios and excellent electrical conductivity. In silicon-based anodes, CNTs function as one-dimensional conductive pathways that enhance the electron transport across the electrode matrix. Their high tensile strength and flexibility also make them suitable for reinforcing the mechanical integrity of the composite. When uniformly dispersed, CNTs create a three-dimensional conductive network within the anode material. This network not only improves the overall electrical conductivity but also facilitates lithium-ion diffusion by providing interconnected

DOI: 10.54254/2755-2721/2025.GL29304

channels. Moreover, CNTs help alleviate the stress induced by silicon expansion through their elastic and hollow structure, which can partially absorb the volumetric strain during cycling. In many designs, CNTs are used in combination with carbon coatings or amorphous matrices to further stabilize the electrode and enhance its electrochemical performance. Due to their structural versatility and multifunctional properties, CNTs are considered one of the most effective carbon additives for improving both the mechanical durability and the charge transport capabilities of silicon anodes. Their compatibility with various fabrication techniques also makes them attractive for scalable manufacturing of high-performance lithium-ion batteries.

3. Analysis & challenge

3.1. Si-Amorphous carbon anode

According to Wang et al., nano-silicon (Si) particles were encapsulated by an amorphous-carbon shell containing fullerene-like fragments (a-C:FL) using a home-made rotating-drum physical vapor deposition (PVD) / DC-pulse magnetron sputtering process [8]. The a-C:FL coating "trapped" curved graphitic planes via sp^3 bonding within an amorphous matrix, combining rigidity and elasticity to disperse stress and preserve Si integrity during cycling. Materials analyses reported nanometer-scale ordered domains in a-C:FL (contrasting with featureless a-C), consistent with higher sp^2/sp^3 ratios and distinct Raman features; these microstructural signatures rationalized improved mechanical response and interfacial behavior. As depicted in Figure 1, the TEM/Raman/XPS panels in the source article visualized curved planes, sp^2/sp^3 evolution, and domain ordering that underpinned the rigid-flexible coupling concept.

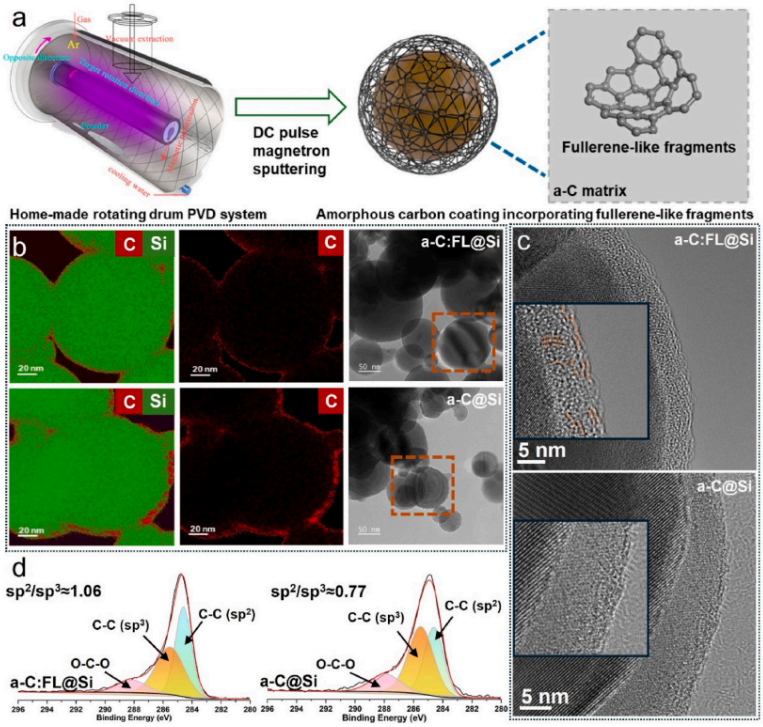

Figure 1. Schematic/TEM/Raman/XPS evidence for fullerene-like fragments embedded in amorphous carbon (a-C:FL), higher sp^2/sp^3 ordering, and a LiF-rich, high-modulus SEI associated with improved stability [8]

DOI: 10.54254/2755-2721/2025.GL29304

The a-C:FL@Si anode delivered strong rate and cycling figures in lithium half-cells, including 1,270 mAh g^{-1} at 5 A g^{-1} and ~1,370 mAh g^{-1} after 100 cycles at 1 A g^{-1}, while maintaining a uniform, smooth, and LiF-rich solid-electrolyte interphase (SEI) with high and homogeneous modulus. The article attributed durability to the synergy between fullerene-like domains and sp^3 anchoring, which acted as "molecular springs," limiting crack initiation and propagation at the carbon/Si and SEI interfaces. These interfacial/mechanical advantages aligned with the measured spectroscopic indicators of higher graphitization (lower ID/IG) and with the model that lower sputtering yield and controlled relaxation time favored structural re-organization into fullerene-like motifs that better accommodated stress [8].

While a-C:FL addressed pulverization and unstable SEI, several risks remained for scale-up. First, the coating window appeared sensitive to plasma power, sputtering yield, relaxation time, and mild plasma heating; these variables altered sp^2/sp^3 and domain ordering, implying tight process control in manufacturing. Second, vacuum PVD infrastructure added cost and imposed throughput limits relative to slurry-based carbon strategies. Third, although the interphase was LiF-rich and mechanically robust, high-temperature operation and pairing with high-voltage cathodes should be validated to exclude latent impedance growth or gas evolution. Finally, the initial Coulombic efficiency (ICE) improvement was not the dominant focus of the report, suggesting that practical cells may still require prelithiation or electrolyte additives to mitigate early Li loss.

3.2. Si-Graphene anode

Fu et, al. prepared SiO/graphene/pitch-carbon composites (SGC-x, x=graphene wt%) by vigorous mixing of commercial SiO (~5 μm), aqueous graphene slurry, and pitch, followed by spray drying and 850 °C/6 h heat treatment in N_2 [9]. Pitch-pyrolytic carbon was used as an interfacial adhesion component to compensate for defects and weak sheet-to-sheet adhesion in macro-graphene assemblies, providing a hybrid that combined rigid carbon (strong C-C bonds) with elastic sliding among graphene layers. The process reconstructed spherical secondary granules in which graphene/pitch-C shells wrapped SiO, enabling enhanced conductivity, compressibility, and a tailored surface area/tap-density balance suitable for industrial electrode calendering.

The study selected SiO@C, SGC-7, SGC-13, and SGC-19 to map how graphene content altered reaction thermodynamics and kinetics. With increasing graphene, reduction peaks shifted to lower potentials without a corresponding oxidation-peak change, indicating that the effect was not dominated by polarization but rather by conductivity gains and a "mechanical-inhibition" interaction that moderated Li uptake into SiO. Reversible capacity and ICE decreased with higher graphene loading (e.g., SiO@C 1643 mAh g^{-1}, 73.1% vs SGC-19 1244 mAh g^{-1}, 68.6%), whereas cycle stability improved markedly (capacity retention after 500 cycles at 1 C: SiO@C 44.9% vs SGC-19 86.2%). The powders also exhibited increased compressing density at elevated loads, despite a general rise in specific surface area with graphene fraction, an effect the authors ascribed to the hierarchical structure and graphene's solid-lubricant behavior. As Figure 2, the source figures collected voltage profiles, rate/long-life data, and property panels that supported these claims [9].

DOI: 10.54254/2755-2721/2025.GL29304

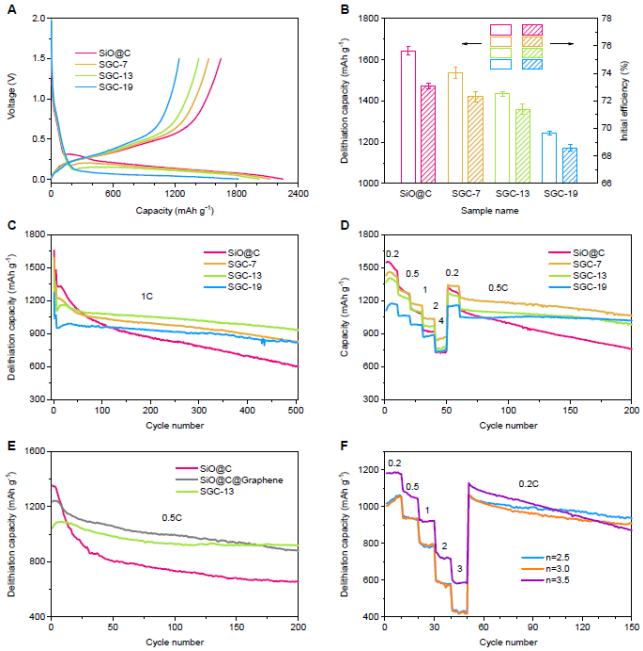

Figure 2. Process schematic and property/electrochemistry panels for SGC-x: lower cathodic peak positions, capacity/ICE vs graphene loading, 500-cycle retention trends, and compressibility/SSA behavior at higher graphene fractions [9]

The "self-mechanical inhibition" perspective explained how graphene shells constrained SiO expansion at both particle and electrode scales, thereby suppressing cracking and slowing resistance growth. However, trade-offs emerged: higher graphene fractions diluted reversible capacity and ICE due to graphene's lower capacity and added surface area; therefore, optimizing the graphene/pitch-C ratio was essential to prevent accelerated fade observed at excessive graphene content. From a manufacturing viewpoint, raised SSA and lowered true/tap density with increasing graphene demanded co-optimization of slurry rheology, calendering pressure, and electrolyte wetting to ensure ionic accessibility in thick electrodes. Finally, while the study demonstrated clear half-cell benefits and mapped property trends, translating this architecture to high-areal-loading, lean-electrolyte full cells would require tight control of particle-size distribution and binder systems to maintain the inhibition effect during long-term cycling.

3.3. Si-Carbon Nanotube (CNT) anode

Huang et al. exploited the explicit nature of magnetron sputtering to deposit elemental silicon directly onto commercial multi-walled carbon nanotube (MWCNT) tissue, creating flexible, free-standing Si/MWCNT anodes [10]. Cross-sectional SEM and EDS mapping confirmed a conformal Si layer with an average thickness of ~427 nm on the outer surface and negligible Si (~0.1 wt%) within inner fiber layers, indicating top-biased utilization inherent to line-of-sight deposition. The authors also discussed van der Waals-driven fiber bundling differences between top and inner layers and noted native surface oxidation of sputtered Si, both of which could influence interfacial chemistry and transport in practical electrodes. As highlighted in Figure 3, the micrographs and elemental maps visualized the coating distribution and the Si-MWCNT interface.

DOI: 10.54254/2755-2721/2025.GL29304

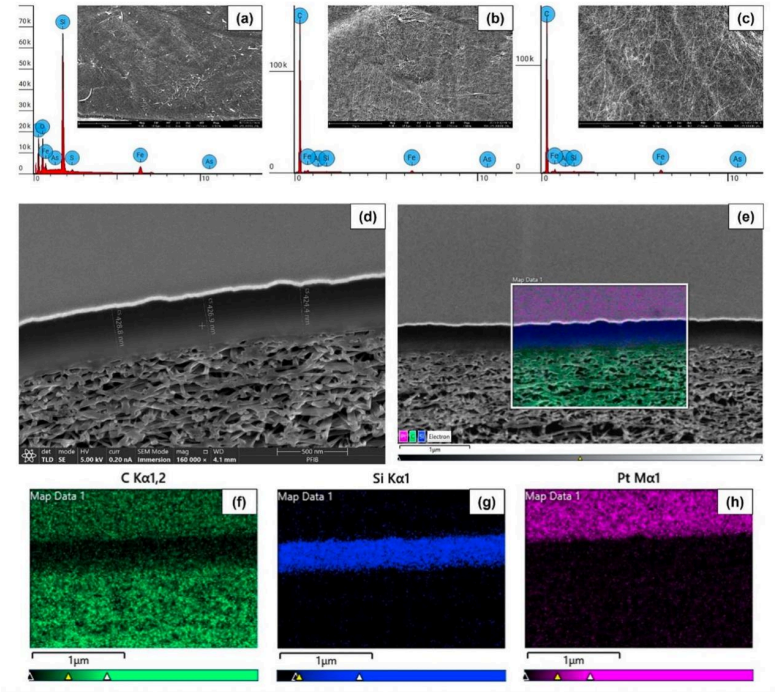

Figure 3. SEM/EDS panels for Si/MWCNT tissue: top-surface vs inner-layer morphology/Si content, and cross-sectional mapping of the Si-MWCNT interface showing a conformal ~427 nm coating localized near the outer surface [10]

Relative to pristine MWCNT tissue (first-cycle CE ≈ 12% rising to ~ 80% by cycle 10; gravimetric capacity ~ 109 mAh g^{-1} at 0.07 mA cm^{-2}, 0.001-2.5 V), the Si-modified fabric exhibited clear morphology and interfacial changes, a conformal ~ 427 nm Si top layer and altered fiber bundling with a well-resolved Si-MWCNT interface, that supported higher utilization and lower interfacial resistance in Li-ion half-cells [10]. First-cycle CE increased to ≈ 23% and reached ~ 94% by cycle 10, while the average gravimetric capacity rose to ~ 290 mAh g^{-1} over 100 cycles; capacity retention improved (C_{100}/C_3 ≈ 39% for Si/MWCNT vs 31% for pristine) under the same 0.07 mA cm^{-2}, 0.001-2.5 V protocol [10]. Cross-sectional composition reinforced the top-biased utilization: surface Si ~27.7 wt% versus ~ 0.1 wt% in inner layers (line-of-sight deposition), and the cumulative "dead-Li" after 100 cycles decreased from ~0.66 mg (pristine) to ~ 0.54 mg with the Si overlayer. Consistently smaller charge-transfer semicircles in early-cycle EIS (cycles 1-10) indicated a lower R_ct for Si/MWCNT than for pristine tissue, aligning with the continuous Si-MWCNT pathways and suppressed SEI growth inferred from the structural panels. As indicated in Figure 3, the SEM/EDS cross-sections and maps provided the necessary context for understanding these kinetic advantages .

Despite its simplicity and compatibility with flexible, current-collector-free formats, the sputter-coated Si/MWCNT concept faced three practical challenges. First, non-uniform depth utilization: line-of-sight deposition concentrated Si on the top surface, leaving inner fibers under-utilized, which could cap areal capacity unless 3D infiltration or graded coatings were engineered. Second, narrow loading window and interfacial stability: thicker Si films would magnify volume swings and SEI re-formation, whereas thinner films would under-protect the MWCNT surface; careful tuning of thickness and post-treatments (e.g., artificial SEI) would be required (a point consistent with broader Si/CNT literature referenced by the authors). Third, manufacturing variability: CNT tissues typically contain catalyst residues (e.g., Fe) and exhibit batch-to-batch differences in fiber bundling, which

DOI: 10.54254/2755-2721/2025.GL29304

could affect long-term reproducibility; native Si oxidation on exposure further complicates electrolyte-interphase formation. Figure 3 in the source paper directly illustrated the coating uniformity and compositional cues motivating these considerations.

4. Summary and suggestion

Table 1. Comparation of various silicon-carbon electrodes

Type	advantages	disadvantages
Si-Amorphous Carbon anode	-crack-tolerant, -LiF-rich SEI -low resistance, -strong rate/cycle	-complex PVD process -power/temperature-sensitive, -scale-up issue -modest areal loading
Si-Graphene anode	-stable shell -higher conductivity -swelling suppression ability -full-cell evidence	-Low capacity -ICE dilution, -accelerated fade,
Si-CNT anode	-simple coating process -early CE rise -lower resistance, -high capacity	-non-uniform utilization -narrow loading window -big first-cycle irreversible loss

The advantages and disadvantages of Si-C was concluded and shown in Table.1. The a-C:FL shell with mixed curved planes and strong sp^3 anchoring stabilizes silicon against cracking, promotes a LiF-rich, uniform SEI, lowers interfacial charge-transfer resistance, and sustains strong rate/cycle performance. The main drawbacks are process-driven: vacuum PVD routes are sensitive to power/temperature history, which complicates scale-up; reported data are often at modest areal loading and require validation in lean-electrolyte, high-loading full cells; and the system can still benefit from prelithiation or targeted additives. Suggestion: keep the a-C concept but push manufacturability. Pilot a roll-to-roll PVD/PECVD line with in-situ thickness/temperature metrology; explore graded a-C shells (outer sp^2 for conductivity, inner sp^3 for anchoring) and light N/B doping to tune elasticity and SEI chemistry; pair with high-efficiency prelithiation and F-rich electrolyte packages (e.g., FEC/VC) to boost ICE; and, critically, qualify at ≥3-4 mAh cm^{-2}, E/S ≤2-3 g Ah^{-1}, and calendered electrodes to demonstrate relevance for practical cells.

Spray-drying followed by ~850 °C treatment yields graphene/pitch-carbon shells around Si/SiO_x, delivering a sharp jump in electronic conductivity and a "self-mechanical inhibition" effect that suppresses swelling; these benefits already have full-cell evidence. Yet, excess graphene dilutes capacity and ICE, can accelerate fade, and typically lowers tap density; at high areal loading the slurry must be co-optimized for wetting and polarization. Suggestion: cap the graphene fraction and let pitch-derived carbon carry density/adhesion, optimize the graphene:pitch ratio (e.g., single-digit to low-teens wt% graphene) and shell thickness to balance elasticity and Li^+ access; raise solids loading (>60 wt%) with rheology control (CMC/SBR + alginate or PU binders), then calender to target porosity (~25-30%) for ionic transport; use mild defect-engineering or few-layer graphene to sustain conductivity while limiting SEI area; and include staged prelithiation to recover ICE without oversizing the negative electrode. A structured DOE on ratio/thickness/porosity will quickly locate the sweet spot at high loading.

Sputter-coating Si onto free-standing CNT tissue is straightforward and yields rapid early CE rise, lower R_ct, and 2-3× capacity versus pristine MWCNT. However, utilization is non-uniform,

DOI: 10.54254/2755-2721/2025.GL29304

the optimal Si loading window is narrow, and first-cycle irreversible loss can be large. Suggestion: upgrade from line-of-sight sputtering to conformal methods (ALD/ICP-assisted or oblique-angle sputter with substrate motion) and nucleation-seeding to even out Si deposition through the fabric thickness; implement a Si/SiO_x gradient or nanolaminate to moderate swelling; apply an artificial, LiF-rich interphase (e.g., very thin $LiPO_x$/LiF or polymer-inorganic hybrid) to curb first-cycle loss; and laminate the fabric onto a thin metal current collector to control impedance while preserving flexibility. Validate at industrially relevant porosity and lean electrolyte, then map uniformity with cross-sectional EDS/Raman to correlate microstructure with utilization.

Across all three routes, the near-term wins are (i) manufacturability at high areal loading with lean E/S, (ii) ICE and fade control via deliberate interphase engineering and prelithiation, and (iii) data-driven co-optimization of shell thickness, carbon ratio, and porosity under full-cell constraints. Medium-term, converge the best elements, graded a-C shells (scale-tolerant), limited-graphene/pitch frameworks (conductive yet dense), and conformal Si deposition on structured scaffolds, into hybrid designs that keep inactive mass low while enabling >80% silicon-rich active fractions. Standardize testing against a high-Ni cathode (e.g., NMC811), report energy at the cell level, and incorporate recyclability and cost in the gate criteria. This combination of scale-ready coating, interphase control, and rigorous full-cell validation is the clearest path to move Si-C anodes from promising lab results to bankable, high-loading industrial electrodes.

5. Conclusion

This study examined silicon-carbon anodes built on three carbon frameworks, amorphous carbon shells (a-C:FL), graphene/pitch-carbon shells, and Si sputtered on CNT fabrics, linking structure and interface design to electrochemical performance and scale-up feasibility under high-loading, lean-electrolyte full-cell constraints. The analysis shows that a-C:FL shells with mixed curved planes and strong sp^3 anchoring are the most balanced pathway, simultaneously enabling LiF-rich, low-impedance interphases, crack tolerance, and robust rate/cycle behavior while remaining compatible with manufacturing. First, it is recommend prioritizing an engineering package centered on graded a-C shells, high-solids slurry and calendering, and efficient prelithiation/SEI control, targeted to practical metrics (≥3-4 mAh cm^{-2}, low E/S) to secure cell-level energy and durability. Second, alternative routes remain valuable but require focused co-optimization: for graphene/pitch systems, cap graphene content and tune shell thickness/porosity to avoid capacity and ICE dilution while preserving conductivity and tap density; Finally, for CNT fabrics, improve deposition uniformity (beyond line-of-sight sputtering) and apply artificial LiF-rich interphases to reduce first-cycle loss and widen the viable loading window. Taken together, these directions map a credible transition from promising half-cell data to bankable, high-loading industrial electrodes, and point to hybrid designs that merge graded a-C stability, controlled graphene conductivity, and conformal Si on structured scaffolds for the next generation of Si-C anodes.

References

[1] Xiao, Z., Wang, C., Song, L., Zheng, Y., & Long, T. (2022). Research progress of nano-silicon-based materials and silicon-carbon composite anode materials for lithium-ion batteries. Journal of Solid State Electrochemistry, 26(5), 1125-1136. https: //doi.org/10.1007/s10008-022-05141-

[2] Cheng, Z., Lin, H., Liu, Y., Yan, Q., Su, B.-L., & Zhang, H. (2025). A Stress-Buffering Hierarchically Porous Silicon/Carbon Composite for High-Energy Lithium-Ion Batteries. Advanced Functional Materials, Article 2505207. https: //doi.org/10.1002/adfm.202505207

DOI: 10.54254/2755-2721/2025.GL29304

[3] Yu, P., Li, Z., Zhang, D., Xiong, Q., Yu, J., & Zhi, C. (2025). Hierarchical Yolk-Shell Silicon/Carbon Anode Materials Enhanced by Vertical Graphene Sheets for Commercial Lithium-Ion Battery Applications. Advanced Functional Materials, 35(2), Article 2413081. https: //doi.org/10.1002/adfm.202413081

[4] Zhang, Q., Yang, Y., Wang, D., Zhang, R., Fan, H., Feng, L., Wen, G., & Qin, L.-C. (2023). A silicon/carbon/reduced-graphene composite of honeycomb structure for high-performance lithium-ion batteries. Journal of Alloys and Compounds, 944, Article 169185. https: //doi.org/10.1016/j.jallcom.2023.169185

[5] Shi, H., Wang, J., Wang, C., Wang, Z., Wang, Z., Chen, X., Li, J., Bai, Z., Gao, Y., & Yan, X. (2024). Design of Supported-Coated Structure Silicon/Carbon Composites Using Industrial Waste Micrometer-Sized Silicon for an Advanced Lithium-Ion Battery Anode. Energy & Fuels, 38(9), 8306-8316. https: //doi.org/10.1021/acs.energyfuels.4c00562

[6] Yang, R., Li, C., Li, X., Zhang, G., Liu, Y., & Deng, J. (2023). Silicon/Carbon Nanoparticles Assembled with Multifunction Carbon Nanotubes/Sheets as High-Performance Anode of Lithium-Ion Batteries. Batteries (Basel), 9(9), Article 460. https: //doi.org/10.3390/batteries9090460

[7] Xu, H., Mu, X., Chen, S., Xu, X., Huang, T., & Yu, A. (2025). Low-cost scalable nano silicon embedded starch-resin crosslinked hard carbon for lithium-ion battery anodes. Journal of Power Sources, 629, Article 236065. https: //doi.org/10.1016/j.jpowsour.2024.236065

[8] Wang, Z., Li, G., Wang, D., & Zhang, B. (2025). Fullerene-like fragments regulated rigid-flexible coupling amorphous carbon coating to stable silicon anode. Materials Today Energy, 53, Article 101978. https: //doi.org/10.1016/j.mtener.2025.101978

[9] Fu, R., Ji, J., Yun, L., Jiang, Y., Zhang, J., Zhou, X., & Liu, Z. (2021). Graphene wrapped silicon suboxides anodes with suppressed Li-uptake behavior enabled superior cycling stability. Energy Storage Materials, 35, 317-326. https: //doi.org/10.1016/j.ensm.2020.11.027

[10] Huang, S., Fedorov, R. G., & Ein-Eli, Y. (2024). Silicon-coated multi-walled carbon nanotube (MWCNT) tissues as flexible free-standing anodes for advanced Li-ion batteries. Journal of Solid State Electrochemistry, 28(7), 2139-2149. https: //doi.org/10.1007/s10008-023-05737-x